หอสมุดกลาง สถาบันวิทยบริการ
จุฬาลงกรณ์มหาวิทยาลัย

CHAPTER II

INFLUENCE OF WEAK ELASTICITY OF DISPERSED PHASE ON DROPLET BEHAVIOR IN SHEARED POLYBUTADIENE/POLY(DIMETHYL SILOXANE) BLENDS

[Wanchai Lerdwijitjarud, Ronald G. Larson, Anuvat Sirivat, and Michael J. Solomon, "Influence of weak elasticity of dispersed phase on droplet behavior in sheared polybutadiene/poly(dimethyl siloxane) blends",
J. Rheol. 47 (1), 37-58 (2003).]

INFLUENCE OF WEAK ELASTICITY OF DISPERSED PHASE ON DROPLET BEHAVIOR IN SHEARED POLYBUTADIENE/POLY(DIMETHYL SILOXANE) BLENDS

SYNOPSIS

The contribution of weak droplet-phase elasticity is investigated for blends of polybutadiene in poly(dimethyl siloxane) in a simple shearing flow with droplet-phase Weissenberg number, Wi_d, up to around unity. The elasticity of the polybutadiene dispersed phase is varied by adding various amounts of high-molecular-weight polybutadiene into low-molecular-weight polybutadiene Newtonian fluid. To isolate the contribution of elasticity, the experiments are conducted at fixed viscosity ratio by varying the experimental temperature to counteract the small effect of high-molecular-weight polymer on droplet viscosity. Droplet deformation and relaxation are measured using an optical flow cell mounted on an optical microscope. As the droplet-phase elasticity increases, the steady-state shape deformation at fixed capillary number, Ca, decreases and the critical capillary number for droplet breakup increases. For a 20%-dispersed phase blend, the steady-state capillary number calculated from the volume-averaged droplet diameter increases with increasing droplet-phase elasticity, but is smaller than for an isolated droplet, suggesting that coalescence has little effect on droplet size in these experiments. However in startup of shear flow, the elasticity of the droplet does not affect the droplet shape, either during the startup of shear flow or during the relaxation process after the startup of shear flow for ratios of Wi_d/Ca up to 0.033.

INTRODUCTION

Properties of immiscible polymer blends depend not only upon the properties of their constituent components but strongly on their morphology as well. For instance, the impact strength of polymer blends can be drastically improved when the rubbery dispersed phase size is below a critical value [Wu (1985)]. The final morphology of polymer blends mainly results from the deformation, relaxation, breakup, and coalescence of the dispersed phase induced by the flow field inside the processing equipment used to shape the polymer product. Thus, an improved understanding of the effect of these processes on blend morphology would obviously be valuable for better controlling the final properties of polymer blends.

Two experimental flow histories have been used to study the behavior of isolated droplets under well-defined flow fields. The first approach is to investigate the steady-state shapes of deformed droplets and the critical conditions required for breaking droplets under steady shear flow [Taylor (1932,1934), Grace (1982), Elmendrop and Maalcke (1985), Elmendrop (1986), Mighri *et al.* (1997,1998), Guido and Villone (1998), Tsakalos *et al.* (1998)]. The other approach is to use step-strain experiments, wherein the effects of material and flow parameters on the transient droplet deformation and shape relaxation are studied [Tsakalos *et al.* (1998), Yamane *et al.* (1998), Almusallam *et al.* (2000), Hayashi *et al.* (2001a, 2001b)].

The steady-state deformation and breakup of a Newtonian drop immersed in another Newtonian fluid were first studied by Taylor (1932,1934). For steady simple shearing flow in the small-deformation limit, Taylor noted that droplet deformation is controlled by two dimensionless parameters, the capillary number, Ca, and the viscosity ratio, η_r. Ca is defined as the ratio between the matrix viscous stress, $\eta_m\dot{\gamma}$, and the interfacial stress, Γ/r_o, where $\dot{\gamma}$, Γ and r_o denote applied shear rate, the interfacial tension between dispersed and matrix phase, and the radius of the undeformed spherical droplet, respectively. η_r is defined as the ratio η_d/η_m between the viscosities of the dispersed (η_d) and the matrix (η_m) phase. In the case of small Ca, the droplet is gradually deformed and reaches a steady-state ellipsoidal shape in

which the major axis of the ellipsoid orients at a certain angle, θ, with the flow direction. At steady-state for small Ca, Taylor found that the orientation angle, θ, is equal to 45° and a deformation parameter, Def, depending on Ca and η_r:

$$Def \equiv \frac{a-b}{a+b} = Ca \frac{19\eta_r + 16}{16\eta_r + 16} \quad \text{.....(1)}$$

where a and b are, respectively, the lengths of the major and minor axes of the deformed droplet. Guido and Villone (1998) reported that the steady-state three-dimensional shape of a droplet under simple shear flow was well described by an ellipsoid having three different principal axes, in which the steady-state length of the minor axis of the ellipsoid in the vorticity direction was larger than that in the shear-gradient direction.

When Ca increases, the droplet deformation increases until Ca reaches a critical value, Ca_{crit}, where the droplet cannot preserve a steady-state ellipsoidal shape. At Ca_{crit}, the ellipsoidal droplet transforms to a sigmoidal shape in which the central part of the sigmoid stretches and simultaneously becomes thinner with applied strain. After a critical strain is reached, the droplet breaks into smaller droplets. From experimental studies of isolated Newtonian droplets sheared in Newtonian matrices [Grace (1982), De Bruijn (1989)], it is found that the minimum Ca_{crit} is obtained when the viscosity ratio is around unity.

The deformation and relaxation of isolated droplets have also been studied in step-strain experiments. In these experiments, the deformation and relaxation behavior can be separately monitored. Yamane *et al.* (1998), and Hyashi *et al.* (2001a) studied the shape recovery after application of large step strains applied to droplets in immiscible polymer matrices for blends with viscosity ratio less than one. A flat ellipsoidal shape was observed just after imposition of a moderate step strain (γ =1-5 units). Subsequently, the droplet relaxes back to a spherical droplet through a series of intermediate shapes, i.e. cylindrical, dumbbell, and ellipsoid of revolution. The evolution is driven by the tendency toward reduced interfacial area. The length of the major axis of the ellipsoid was observed to be slightly larger than that predicted by affine deformation; however, the orientation angle data of this axis with

respect to the flow-vorticity plane was in good agreement with that predicted by affine deformation. Step-strain experiments for Newtonian blends with viscosity ratio around one were also investigated by Almusallam *et al.* (2000). A phenomenological constitutive model, modifying the Doi-Ohta theory [Doi and Ohta (1991)], was constructed which predicted transient stresses and ellipsoid shapes in terms of the droplet anisotropy tensor. The droplet anisotropy tensor during relaxation after step strain was quantitatively described by this model for moderate strains (γ = 1-5). Droplet behavior under application of reversing step shear strains [Guido *et al.* (2000)] and large double-step shear strains [Hayashi *et al.* (2001b)] has also been recently reported.

For a viscoelastic drop immersed in a viscoelastic matrix such as in commercial polymer blends, the elastic properties and shear-thinning of the blend components, in addition to their viscous properties, may influence droplet behavior during shear flow. Elmendorp and Maalcke (1985) studied the contribution of elasticity to the breakup of isolated viscoelastic drops in Newtonian matrices and of Newtonian drops in viscoelastic matrices in simple shear flow. They found that the more elastic droplets (as measured by the first normal stress difference N_1) were the more stable against breakup, while the more elastic matrices led to increasingly unstable droplets, all else being equal. Levitt *et al.* (1996) observed drop widening in the neutral direction of the shear flow when isolated drops of polypropylene were sheared in a high-elasticity polystyrene matrix. They proposed that the width of the flattened drops was dependent upon the difference in storage modulus between the matrix and the droplet phase. Mighri and co-workers investigated the influence of elasticity contrast, as measured by the ratio λ_d/λ_m of the relaxation time of the droplet phase, $\lambda_d \equiv N_{1d}/2\eta_d\dot{\gamma}^2$, to that of matrix phase, $\lambda_m \equiv N_{1m}/2\eta_m\dot{\gamma}^2$, on isolated droplet deformation in an elongational flow [Mighri *et al.* (1997)] and on isolated droplet deformation and breakup in a shear flow [Mighri *et al.* (1998)]. Here, N_{1d} is the first normal stress difference of the droplet phase and N_{1m} is that of the matrix phase. They found that the drop deformation diminished as the drop/matrix relaxation-time ratio increased in either the elongational or shear flows. In a shear flow, when $\lambda_d/\lambda_m < 4$, the value of Ca_{crit} at which droplet breakup occurs drastically increased with

increasing λ_d/λ_m; but for $\lambda_d/\lambda_m > 4$, it did not change much further. Although most experimental data in the literature suggest that droplet-phase elasticity leads to less deformed, more stable, droplets relative to comparable Newtonian droplets, studies of droplet behavior when droplet elasticity is the sole manipulated valuable are rare, since in most previous work both droplet elasticity and viscosity ratio were varied simultaneously.

This paper is, therefore, devoted to the investigation of the influence of droplet elasticity on droplet behavior in a shear flow using blend systems at fixed viscosity ratio. Specifically, the steady-state deformed shape, Ca_{crit}, and the shape deformation and shape relaxation after startup of shear flow for an isolated droplet in a matrix with the same viscosity as the droplet fluid, but different dispersed-phase elasticities (as measured by the first normal stress difference, N_1) were measured.

EXPERIMENTAL METHODS

A. Materials

The materials used in this study were polydimethylsiloxane, PDMS (GE VISCASIL 100M donated by General Electric) as the matrix phase and polybutadiene, PBd (Ricon 150 donated by Ricon Resin Inc.,CO) as the dispersed phase. The properties of the blend components are listed in Table 2.1. High-molecular-weight polybutadiene (MW 1.65 x 10^5, polydispersity 1.05 purchased from Polymer Source Inc., Canada) was also used as a dilute high molecular weight polymer component added to the Ricon 150 to make a "Boger" fluid [Boger and Binnington (1977)] with significant elasticity but not much shear thinning.

B. Components and Blend Preparation and Characterization

- *Preparation and characterization of blend components*

PDMS was used as received. Since the Ricon 150 contained some volatile components as received, fresh Ricon 150 was vacuum dried at 50°C until the weight loss ceased and all volatile components were driven off. The "Boger" polybutadiene dispersed phase was prepared by completely dissolving a few tenths of a percent of high molecular weight polybutadiene into methylene chloride. The solution was gently mixed with low-molecular-weight Newtonian polybutadiene, Ricon 150, at room temperature for at least 5 days to obtain a homogenous solution. The mixture was subsequently dried in a vacuum oven at 50 °C to remove the methylene chloride carrier solvent and any other volatile substances until no further weight change was observed. The steady-state viscosity and first normal stress difference of each blend component was measured by a cone-and-plate rheometer (Rheometrics Scientific, model ARES, NJ) (25-mm plate diameter with cone angle 0.1 rad.). Figure 2.1 shows the viscosities and first normal stress differences of all PBd solutions at 21.0 °C. Pure PBd shows Newtonian behavior, whereas weak shear thinning and weak elasticity, the latter indicated by a small value of the first normal

stress difference N_1, were detected in the PDMS at high shear rates (see Fig. 2.2). The dependence of the zero-shear viscosity, η_0, on the concentration of high-molecular-weight PBd in the PBd Boger fluids is also given in Figure 2.1. Due to the influence of the high-molecular-weight polybutadiene, both η_0 and N_1 of the solution increase with concentration of high-molecular-weight polymer. For the solutions containing 0.1% and 0.2% high-molecular-weight polymer, the increment in the zero-shear viscosity over that of pure Ricon 150 is approximately proportional to the concentration of high-molecular-weight polymer, indicating that these solutions are dilute in high-molecular-weight PBd. An upward curvature of η_0 with increasing percentage of high-molecular-weight PBd, particularly evident for the 0.5% solution, can be attributed to the onset of the entanglement effects. Since the temperature-dependence of the viscosities of PDMS and PBd are different, a condition of nearly equal viscosities of the PBd fluids with the PDMS could be established for each blend by adjusting the temperature. The constituent components, the temperature at the equi-viscosity condition, and the stress ratios ($S_{Ri} \equiv N_{1i}/(\eta_i\dot{\gamma})$) at a shear rate of 10 s^{-1} for the matrix and dispersed fluids for all blends studied are tabulated in Table 2.2. Figure 2.2 shows the steady shear viscosity and first normal stress difference of each fluid pair at the temperature in which both matrix and droplet fluid have the same viscosity. Because of the modest shear thinning of the 0.5% PBd Boger fluid, perfect matching of the viscosities at this fluid could only achieved at a single shear rate.

As shown in Figure 2.2, the viscosity ratio of all fluid systems studied are comparable ($\eta_r \approx 1$), but the difference between N_1 of the droplet phase and that of the matrix phase increases from fluid system A1 to A4. The storage modulus (G') and loss modulus (G") data in the linear viscoelastic regime of all PBd solutions are shown in Figure 2.3. The effective relaxation times ($\tau_{eff,d} = \Psi_{1,0}/(2\eta_0)$, where $\Psi_{1,0} = 2\eta_0^2G'/[G"]^2$) of all PBd solutions were calculated using G' and G" data from the terminal regime. The relaxation time of the high-MW PBd contribution ($\tau_{eff,p,d} = \Psi_{1p,0}/(2\eta_{p,0})$, where $\Psi_{1p,0}$ and $\eta_{p,0}$ are the contribution of high-MW PBd to the zero-shear first normal stress coefficient, $\Psi_{1,0}$, and zero-shear viscosity, η_0, of PBd solutions respectively) of all PBd solutions are also calculated. Both $\tau_{eff,d}$ and $\tau_{eff,p,d}$

are listed in Table 2.2. The first normal stress difference of dispersed phase estimated from G' and G" in the terminal regime are presented in Figure 2.2.

- *Preparation of concentrated blend*

All concentrated blends studied contain 80% by weight PDMS matrix-phase fluid and 20% by weight dispersed PBd. Constituent component fluids were weighed and then mixed with a spatula for around 20 min. until white-creamy samples were obtained. The air bubbles generated during the mixing step were removed by leaving the blend at rest at ambient conditions for four hours before further use.

C. Optical Microscopy of an Isolated Droplet

A flow cell (Linkam CSS 450, Linkam Scientific Instruments Ltd., UK) with parallel disk geometry attached to an optical microscope (Olympus BX50, Olympus America Inc., NY) was used to study the deformation and relaxation of an isolated droplet of PBd under shear. Images were captured in the flow-vorticity plane by using a CCD camera (Cohu 4910, Cohu Inc., CA). NIH-image software (U.S. National Institutes of Health, available at http://rsb.info.nih.gov/nih-image) was used to process the images.

The matrix phase was loaded into the flow cell and various single droplets were subsequently immersed into PDMS by using a micro syringe. The upper plate of the flow cell was gradually lowered to the desired gap setting. To maintain the equi-viscosity condition throughout the experimental run, the temperature of the flow cell was controlled by a water bath. If the droplet is too close to the wall, the wall exacerbates the deformation of the droplet and also causes the droplet to migrate away from the wall [Kennedy *et al.* (1994); Uijttewall and Nijhof (1995)]. To minimize this effect, the droplet-wall spacing, i.e. h/r_o, where h is the distance of the droplet's center from the closest wall and r_o is the original droplet radius, should be

greater than five. In all our experimental results presented, h/r_o was kept above seven by choosing a droplet located at the center of the gap.

To generate the shearing flow, the lower disk of the flow cell was rotated by using a stepper motor, with the upper disk held fixed. The droplet of interest thus usually moves out of the viewing window as the lower disk is rotated. To bring the droplet into the viewing frame after performing a step strain, the chosen droplet was first driven out of viewing window by applying a relatively small shear rate until the desired magnitude of the subsequent step strain was imposed. Then, the droplet was allowed to completely relax into a spherical shape under quiescent conditions. The same strain in the opposite direction was then applied at the desired high shear rate, thus deforming the droplet and simultaneously bringing it back into view.

Since the images of the deformed droplet were captured only in the plane perpendicular to the shear-gradient direction, the lengths of all three principal axes of the ellipsoidal droplet could not be determined directly. However, the lengths of all three principal axes can be determined from images in the shear-vorticity plane by using the orientation angle (θ), which is the angle of the major axis of the deformed droplet in the flow-flow gradient plane. As verified by previous researchers [Yamane *et al.* (1998); Okamoto *et al.* (1999) and Almusallam *et al.* (2000)], the orientation angle predicted by an affine-deformation model is close to the experimental value for step-strain or start-up flow when Ca is at least three times higher than Ca_{crit} and if the shearing is of sufficient duration. In the case of $Ca \leq Ca_{crit}$, the orientation angle predicted by affine deformation is not suitable to obtain the lengths of the principal axes of the droplet. Chaffey and Brenner (1967) derived the following relation between the orientation angle at steady state and the applied capillary number:

$$\theta = \frac{\pi}{4} - \frac{(19\eta_r + 16)(2\eta_r + 3)}{80(1 + \eta_r)} Ca \qquad \text{..... (2)}$$

This relation was verified by Guido and Villone (1998) by comparing it with the orientation angles obtained by microscopy for polydimethylsiloxane droplets sheared in polyisobutylene at $\eta_r = 1.4$ and 2. Good agreement between the experimental data and equation (2) was obtained. Although the above relationship of Chaffey and

Brenner was derived for Newtonian liquids, our droplets are only weakly elastic, and we will therefore use the orientation angles obtained from Chaffey and Brenner relation to obtain the droplet aspect ratios in our experiments. We note that the elastic effects become larger at increased capillary number, but the droplet also becomes both more extended and more oriented under these conditions, and the deformed droplet aspect ratio therefore becomes less sensitive to small variations in the orientation angle. Hence, our results are not likely to be greatly affected by deviations in the orientation angle from that predicted by Chaffey and Brenner.

Since the orientation angle predicted by affine deformation and Chaffey and Brenner relation are derived for Newtonian system, an attempt to infer the orientation angle of an isolated droplet from rheological measurements on a 20%-dispersed phase blend was made with our system with the highest degree of elasticity (blend system A4). The average droplet orientation during flow can be determined by using the ratio of the interface contribution of first normal stress difference to that of shear stress ($N_{1,excess}/\sigma_{12,excess} = 2\cot(2\theta)$) [Jansseune *et. al.* (2000), see also Almusallam *et al.* (2000)]. The 20%-dispersed phase blend of blend system A4 was subjected to a steady-state shear flow at shear rate of 1.0 s^{-1} for a stain of 20,000 to attain a steady-state droplet size. To verify the angle obtained from the affine prediction, a startup of shear flow (imposed $Ca > 3\ Ca_{crit}$) was then applied to the blend sample. The excess stresses due to the interfacial contribution during the relaxation process were used to determine the orientation angle. The results are in good agreement with affine prediction as shown in Figure 2.4. For $Ca < Ca_{crit}$, the steady-state shear stress and first normal stress difference at a shear rate of 0.7 s^{-1} for blend system A4 after it reached a steady-state morphology were used to determined the droplet orientation angle. The angle deduced from this experiment is 20 degrees, which is close to the value of 24 degrees predicted from the Chaffey and Brenner relation. Therefore, the droplet orientation angles predicted assuming affine deformation for the startup experiments at $Ca > 3Ca_{crit}$ and using Chaffey and Brenner relation for steady-state shear at $Ca < Ca_{crit}$ are reasonably accurate for all blend systems in our experiment.

By using θ predicted either from affine deformation or from Chaffey and Brenner relation coupled with the condition that the droplet volume remains constant

during deformation, the lengths of all three principal axes were determined. The method by which the lengths of the three axes can be extracted from the angle θ and the image in the flow-vorticity plane is given in Almusallam *et al.* (2000).

D. Optical Microscopy of Concentrated Blend

The bubble-free 20% dispersed-phase sample was loaded into the flow cell. The gap between the parallel disks was gradually reduced to 500 μm. The steady-state morphology of the blend samples was obtained by performing a steady shearing flow at the desired shear rate for 20,000 strain units. The blend images were obtained using NIH-Image software and then transferred to a Photoshop program (Adobe Systems, Inc) to outline the droplets. The images were brought back to the NIH-Image software to measure the droplet diameter of each droplet. From the droplet size distributions, the volume-average droplet diameter, D_v, was calculated by using the following equation:

$$D_v = \sum_i \Phi_i D_i \qquad \text{..... (3)}$$

where Φ_i is the volume fraction of the droplets with diameter D_i relative to the total volume of the droplets. Typically, data from 400-600 droplets were used to calculate D_v.

E. Experiments on an Isolated Droplet

- *Determination of interfacial tension from the linear shape relaxation of a single droplet*

The evolution of isolated droplet shape after a step strain was recorded. Semi-logarithmic plots of the droplet deformation parameter, Def, (equ.(1)) versus relaxation time were constructed. The characteristic relaxation time for a single droplet, τ, can be derived from the slope, $-1/\tau$, of a straight line fitted to the data in the linear relaxation regime [Luciani *et al.* (1997), Mo *et al.* (2000), Xing

et al. (2000)]. The interfacial tension, Γ, is then calculated from the Palierne model [Palierne (1990) and Graebling *et al.* (1993); see also Taylor (1932)] in the limit of zero volume fraction of dispersed phase:

$$\tau = \frac{(3+2\eta_r)(16+19\eta_r)r_0\eta_{m,0}}{40(1+\eta_r)\Gamma} \qquad \text{..... (4)}$$

where $\eta_r \equiv \eta_{d,0}/\eta_{m,0}$ is the ratio of zero-shear viscosities of dispersed to matrix phase, and r_o is the radius of the spherical drop. This relation can be used to determine the interfacial tension of viscoelastic materials if the relaxation of the continuum elastic stress of the blend constituents is relatively fast compared with the droplet shape relaxation and the droplet retraction rate is sufficiently slow to ensure that the materials behave as Newtonian during the droplet shape relaxation [Luciani *et al.* (1997), Xing *et al.* (2000)]. The single-droplet relaxation data for each fluid system were used to determine the interfacial tension. The average values of the interfacial tension for all blends studied are tabulated in Table 2.2.

- *Droplet deformation and relaxation after a startup of shear flow*

Droplet shapes after a startup of shear flow were studied. Strains of 3, 6 and 8 were chosen for these experiments. At each strain, an isolated droplet was selected and various shear rates were imposed corresponding to different values of the capillary number for that droplet. To ensure that the droplet dimensions after cessation of flow were captured immediately, fast sequential images were taken at a rate of 30 frames/s.

Shape recovery of an isolated droplet after startup of shear flow was also investigated. To minimize the influence of variations in the droplet size, all droplets chosen for study were of comparable initial radius. Strains of 2.2, 3.0, 4.1 and 5.0 were applied, with the shear rate chosen to be high enough that minimal relaxation of droplet shape occurred during the startup of shear flow. Since the initial diameter of the droplet, the matrix viscosity, and the interfacial tension of each fluid system are slightly different, these applied shear rates were adjusted slightly

from system to system to maintain a constant value of Ca for each applied strain. Table 2.3 lists the parameters used in the droplet-relaxation experiments. To ensure that all shape relaxation zones were recorded, the image capture was begun before the startup of shear flow was applied. The image capture continued first at rates of 15 frames/s and then at rates of 6 frames/s until the droplet completely returned to a spherical shape. The higher rate of capture was used to resolve the early stage of shape recovery, whereas the slower one was used to record images during the remainder of the relaxation process.

- *Steady-state droplet deformation and determination of the critical capillary number*

Steady-state shapes for isolated droplets below the critical capillary number for droplet breakup were also investigated. The strain required to reach a steady-state droplet shape was first determined. The applied shear rate was then gradually increased at a rate slow compared to the inverse of the time required for the droplet shape to come to steady-state at any fixed shear rate. The slow increase in shear rate was continued until the critical shear rate required to break the droplet was reached. For each blend, this critical shear rate was recorded.

F. Experiments on Concentrated Blends

- *Steady-state droplet size and size distribution*

Steady shear flow at a rate of 0.1 s^{-1} was applied to each 20% dispersed-phase blend for 10 hr at the equi-viscosity condition. At this low shear rate, coalescence occurred, resulting in a coarse morphology. The shear rate was then stepped up to 0.3 s^{-1} and continued to a stain of 20,000 units to achieve a steady-state morphology. Subsequently, the flow was stopped to allow the deformed droplets to relax. Due to the high viscosity of matrix phase and low testing temperature of our system studies, the diffusion coefficient due to the Brownian motion is quite low. For a droplet with diameter of 5 μm at 21 ^{0}C, the value of

diffusion coefficient due to the Brownian motion is around 10^{-6} $\mu m^2/s$. The time waiting for droplet relaxation is less than 30 s., thus the coalescence effect during this time period should be negligible. The droplet size distribution was then measured. The shear rate was increased in small steps, i.e. to 0.5, 0.7, 1.0, and 2.0 s^{-1}, from the previous steady-state shear rate. For each shear rate, a strain of 20,000 was allowed for attain a steady-state morphology.

RESULTS AND DISCUSSION

A. Steady-State

- *Steady-state deformation of an isolated droplet ($Ca < Ca_{crit}$) and the critical capillary number (Ca_{crit})*

After a small shear rate is imposed, the droplet moves and deforms simultaneously until after sufficient straining, a steady-state deformed droplet shape is reached. The strain required to attain a steady-state shape increases as the imposed shear rate increases. For all shear rates used for all blends studied, the steady-state shape was obtained within a strain of 30 units. Thus, a strain of 30 was applied before capturing the droplet images.

We approximated the steady-state deformed shape of the droplet by an ellipsoid having three different principal axes *a*, *b*, and *c*, in which the steady-state length of the minor axis of the ellipsoid in the vorticity direction (*c* axis) was larger than that in the shear-gradient direction (*b* axis). The deviation of droplet projection taken from the droplet image from the equivalent ellipse was quantitatively verified by Guido and Villone (1998) for isolated Newtonian polydimethylsiloxane droplet sheared in Newtonian polyisobutylene matrix with viscosity ratio of 1.4. The deviation was essentially zero up to Ca around 0.3 and quite small from Ca 0.3 to 0.4. The deviation was really important only when Ca approached the breakup point. Since our droplets are only weakly elastic, an ellipsoid having three different principal aces is reasonably used to represent a steady-state deformed droplet shape in our experiments. Figure 2.5 depicts the half-lengths of the three principal axes at steady state deformation as functions of imposed capillary number. Figure 2.6 shows the dependence of deformation parameter on applied capillary number for all fluid systems studied at a viscosity ratio $\cong$ 1. At small capillary number, all droplets had similar deformation, while, at higher capillary number, the more elastic droplets deformed less. This result agrees with Mighri *et al.* (1998); however, our experiments with Boger fluid blends at the viscosity ratio of unity unambiguously identify the observed effect as due to the effect of droplet elasticity, rather than

หอสมุดกลาง จุฬาลงกรณ์มหาวิทยาลัย

viscosity ratio. Mighri *et al.* (1998) also found that, when the Newtonian droplet was sheared in a Newtonian matrix ($\eta_r = 0.50$), at low shear rate the shape of steady-state deformed droplet was spheroidal with highly curved ends and changed to an elongated cylinder with highly curved ends at shear rates approaching critical value for breakup. In contrast, when the elastic drop was sheared in the elastic matrix ($\eta_r = 0.28$, $\lambda_d/\lambda_m = 0.07$), a spheroidal shape with slightly shaper edges was obtained at low shear rates and a cylindrical shape with highly pointed ends was obtained at high shear rates. Unlike Mighri's results, no deformed droplet with pointed end was observed in our steady-state deformed viscoelastic droplet images. The difference may be caused by the following reasons; i) although the matrix phase, PDMS, used in our experiments has some elasticity, the elasticity is relatively smaller comparing with that used in Mighri's experiment, ii) the viscosity ratios of all blend systems studied in our experiments are relatively fixed ($\eta_r \sim 1$), whereas in Mighri's experiment the viscosity ratios were varied, i.e. 0.50 for the Newtonian system and 0.28 for the elastic system.

The critical capillary number obtained from our experiments with Newtonian blend constituents was 0.47. This result is comparable to 0.5 and 0.46 which are the values predicted by Taylor's theory [Taylor (1932, 1934)] and De Bruijn's semiempirical relation [De Bruijn, (1989)], respectively. As shown in Figure 2.5, the critical capillary number increases with the elasticity of the droplet, i.e. $Ca_{crit} = 0.52$ for blend A2, $Ca_{crit} = 0.58$ for blend A3, and $Ca_{crit} = 0.62$ for blend A4. These results suggest that the elasticity of the dispersed phase resists the deformation and breakup of the droplet. This result agrees qualitatively with the result reported by Mighri *et al.* (1998), who found that Ca_{crit} increases with increasing the elasticity ratio ($k' \equiv \lambda_d/\lambda_m$), which was defined as the ratio of Maxwell relaxation time of the droplet phase, $\lambda_d \equiv N_{1d}/2\eta_d\dot{\gamma}^2$, to that of the matrix phase, $\lambda_m \equiv N_{1m}/2\eta_m\dot{\gamma}^2$. In the definition of Mighri *et al.*, the elasticity ratio is a combination of both the viscosity ratio and the ratio of first normal stress differences. However, the viscosity ratios of our blend systems are all near unity. Thus, in our experiments, the increase of Ca_{crit} for the non-Newtonain components can be attributed to droplet elasticity alone.

The correlation between Ca_{crit} and droplet-phase Weissenberg number ($Wi_d = \dot{\gamma}_c \cdot \tau_{eff,d}$) is shown in Figure 2.7. The Ca_{crit} increases monotonically with increasing Wi_d. Interestingly, the linear relation between Ca_{crit} and Wi_d is established for the data points of the blend systems A1, A2, and A3, whereas the deviation from linear relation occurs for blend system A4. This result seems to correlate with the fact that blend systems A2 and A3 are dilute solutions of high-MW PBd in Newtonian PBd base fluid (blend system A1), while blend system A5 is beyond the dilute regime (see Figure 2.1). From the linear relation of the first three data of Figure 2.7, an extrapolation to the value of Wi_d of zero gives Ca_{crit} of 0.45, which nearly recovers Grace's result (Ca_{crit} = 0.46) for the a Newtonian blend system with viscosity ratio unity.

- *Steady-state droplet size of concentrated blends*

For a 20% dispersed-phase blend sheared at a given shear rate for a prolonged period after a step-up from a previous shearing at a rate of 0.1 s^{-1}, a dynamic equilibrium between breakup and coalescence is established resulting in steady-state morphology. From the steady-state morphology, the volume-averaged diameters (D_v) of each system were determined. Figure 2.8 displays the steady-state capillary number (Ca_{ss}) calculated from steady-state volume-averaged diameter as a function of applied shear rate for blends A1, A3, and A4. When the elasticity of the droplet phase increases, Ca_{ss} increases for all applied shear rates studied. This result is consistent with previous reports [Elmendorp and Maalcke (1985), Mighri *et al.* (1998)], but the contribution of elasticity effect is more unambiguously identified in our experiment, since the viscosity ratio is held fixed in our experiments.

Comparing Figures 2.6 and 2.8, it is interesting to note that the steady-state capillary number of a 20%-dispersed phase blend is smaller than the critical capillary number for an isolated droplet for the same pair of fluids. Several reasons can be used to explain this observation. The viscosity of an emulsion or an immiscible blend lies above the viscosity predicted by a linear mixing rule in the viscosities of the constituent components [Taylor (1932), Frankel and Acrivos

(1970), Choi and Schowalter (1975)], because of the contribution of the interfacial tension to the emulsion viscosity. Therefore, in a concentrated system, a higher viscous stress can be expected to act on the droplet than in the dilute regime at the same shear rate, resulting in smaller droplets and therefore smaller Ca_{ss}. This phenomenon was also observed by Jansen *et al.* for Newtonian blend systems [Jansen *et al.* (2001)]. They found that the critical capillary number for breakup of a 70% dispersed-phase emulsion is lower than that of isolated droplet by more than an order of magnitude. They proposed the mean-field average model, which uses the emulsion viscosity instead of matrix viscosity, to predict the droplet breakup for an emulsion or concentrated blend.

Here, we choose the Frankel-Acrivos (FA) Model [Frankel and Acrivos (1970)] to predict the viscosity of our blends. Grizzuti *et al.* found good quantitative agreement between this model and their experimental data [Grizzuti et al. (2000)]. The Frankel-Acrivos model is

$$\eta = \frac{\eta_m}{1+\Lambda^2\left(\frac{\eta_m r_0}{\Gamma}\right)^2 \dot{\gamma}^2}\left\{1+\frac{5\eta_r+2}{2\eta_r+2}\phi+\Lambda^2\left(\frac{\eta_m r_0}{\Gamma}\right)^2\dot{\gamma}^2\left[1+\frac{5\eta_r+2}{2\eta_r+2}\phi-\frac{19\eta_r+16}{2(\eta_r+1)(2\eta_r+3)}\phi\right]\right\}$$

where

$$\Lambda = \frac{(2\eta_r+3)(19\eta_r+16)}{40(\eta_r+1)} \qquad \text{..... (5)}$$

Based on the emulsion viscosity predicted from FA model, the Ca_{ss} was recalculated. The detail of the calculated values for blend A1 is also listed in the Table 2.4. A measured value of the blend viscosity is available only for blend system A1, and it is a little higher than predicted by the FA model. Thus, the Ca_{ss} calculated based on these measured values approaches, but remains less than, Ca_{crit} for an isolated droplet, as shown in the Table 2.4.

Another possible reason that Ca_{ss} is less than Ca_{crit} for an isolated droplet is that the flow field surrounding a droplet in a concentrated blend is somewhat more irregular than for a simple shear flow, and an upward fluctuation in velocity gradient could break up droplets to smaller size than would be obtained in a locally steady flow. In addition to the higher viscous stress and the fluctuating flow

field, yet another possible cause for the difference between Ca_{ss} of a concentrated blend and Ca_{crit} of an isolated droplet is the existence of a "dead zone" [Janssen (1993), Minale *et al.* (1997)], i.e. a range of shear rates for which droplets of a certain size range neither breakup nor coalesce. Since the initial morphology was prepared by shearing at 0.1 s^{-1}, the initial droplet diameters are quite large. When shear rate is rapidly stepped up and the applied Ca is larger than about two times Ca_{crit} for droplet breakup, the droplets could be stretched into long cylinders and subsequently break into many smaller droplets due to Rayleigh instabilities [Elmendorp (1986), Janssen (1993), Tsakalos *et al.* (1998)]. Tsakalos *et al.* (1998) showed that the droplet diameter resulting from thread breakup mechanism is approximately one half the critical droplet diameter as predicted by Taylor for their blends. If the resulting droplets fall into the "dead zone", then the sub-critical droplet sizes formed by this break up will not coalesce into larger droplets. Therefore, Ca_{ss} for 20%-dispersed phase blends calculated from the volume-averaged droplet diameter could be lower than Ca_{crit} of isolated droplets.

It is also puzzling that the steady-state capillary number depends weakly on shear rate, even for nearly Newtonian components. In principle, dimensional analysis implies that this steady-state capillary number should be independent of shear rate [Doi and Ohta (1991)], unless another variable enters the problem. Possible candidates for this "extra variable" include the droplet size during the pre-shearing period where the shear rate is 0.1 s^{-1}, some effect of the very weak elasticity of the PDMS matrix phase, or perhaps the small but finite critical thickness of the lubricating layer between droplets at which coalescence occurs.

It is interesting to note that for highly elastic, shear-thinning, melts sheared in commercial mixers, it has been observed that the droplet size of concentrated blends is significantly higher than for isolated droplets, and increases with increasing volume fraction of droplet phase [Sundararaj and Macosko (1995)], a finding that has been attributed to the effects of coalescence. Our results, obtained under well-controlled conditions of steady shearing with fixed viscosity ratio and minimal shear thinning, show the opposite, i.e., smaller droplets in the blends than for isolated droplets. This seems to imply that the larger droplet size obtained in these earlier experiments was not produced by coalescence alone, but was also

influenced by the viscosity ratio, high elasticity, shear thinning, or non-idealities in the flow produced by commercial blenders. The different result we have obtained reinforces the importance of performing well-controlled experiments, if one wishes to sort out the competing effects of the many factors that control blend morphology.

B. Startup of Shear Flow with Isolated Droplets

Droplet relaxation

A flat ellipsoidal shape is initially produced right after an application of startup of shear flow with width in the "*c*" or vorticity direction greater than the thickness of the droplet in the "*b*" or shear gradient direction. The droplet shape during relaxation also depends on the imposed strain. For moderate strains (2 or 3), at the early stage of droplet recovery, the width of the droplet first decreases until both minor axes are comparable in length, whereas the major axis (*a* axis) is relatively constant, so that the droplet shape becomes cylindrical. Subsequently, both *b* and *c* axes continually increase in length, while the *a* axis simultaneously shrinks. The rod-like shape thus transforms into an ellipsoid of revolution. At the final stage of relaxation, the ellipsoid of revolution gradually relaxes back to the original spherical shape. For a higher strain (4 or 5), a dumbbell shape appears at an intermediate stage in time between the rod and the ellipsoid of revolution. These results are similar to those reported earlier [Yamane *et al.* (1998) and Almusallam *et al.* (2000)]. The three principal axes, normalized by the original droplet radius (a/r_0, b/r_0, and c/r_0), are plotted as functions of time normalized by $\Gamma/(\eta_0 r_0)$ for fluid system A1 at various strains in Figure 2.9.

The same experimental procedure was applied to blends A2, A3, and A4. At the same Ca and γ, the shape relaxations of the elastic droplets (A2, A3, and A4) are almost indistinguishable from those of the Newtonian droplet, as shown in Figure 2.10. Unlike the steady-state deformation experiment, there is no effect of dispersed-phase elasticity on the shape relaxation. There are several possible explanations for this. The first possible reason is that all dispersed-phase fluids

investigated have only a Newtonian response during the relaxation process, since the characteristic shear rate of the flow generated during the droplet relaxation is relatively low in this period. The second reason is that the time scale for relaxation of droplet fluid elasticity is very fast compared to the time scale of shape recovery driven by the interfacial tension, and thus the elasticity of the dispersed phase does not affect the droplet-shape relaxation.

- *Droplet deformation*

As noted earlier, a flat ellipsoidal droplet shape was obtained immediately after a startup of shear flow was applied. Figure 2.11 shows the measured lengths of principal axes taken from droplet images immediately after stopping the flow. The applied strain was increased from 3 units (Figure 2.11a), to 6 units (Figure 2.11b), and to 8 units (Figure 2.11c). The greater the applied strain, the more distorted is the droplet shape. For the same imposed strain, the extent of deformation increases with applied capillary number and tends to reach a constant value at high capillary number. As previously reported [Levitt *et al.* (1996)], the drop-widening phenomenon, i.e. that the width of the deformed droplet (c axis) is greater than the original value, was also observed in our experiments for the blends (B1, B3, and B4) in which the viscosity ratio is equal 0.5. The widening phenomenon in Figure 2.11 is evidenced by a ratio c/r_0 exceeding unity, which is only achieved at high Ca for the closed symbols, which correspond to a viscosity ratio of 0.5. It is interesting to observe that for fixed viscosity ratio, the curves for all elastic droplets cannot be discerned from those of Newtonian droplets. Thus the viscosity ratio affects the shape of the deformed droplet, but the elasticity does not, at least for the range of elasticities and strains considered here. Two possible reasons can be involved to explain this phenomenon. One is that the viscous force exerted on the droplet is very high, since we impose a high Ca in these experiments, and the effect of elasticity of the dispersed phase could be swamped by the higher viscous forces. Note that since both the capillary number, Ca, and dispersed-phases Weissenberg number, Wi_d, are proportional to shear rate, the ratio of the two, Wi_d/Ca, is constant for all blends, and its value is small, $Wi_d/Ca = 0.033$, even for the

most elastic droplet fluid used here. Another possible reason for the absence of an elastic effect in the startup experiments (despite its influence on steady-state droplet size) is that the elastic response of viscoselastic materials after startup of shearing flow is normally slow compared to the viscous response. Unlike the steady-state experiments, the strains used in these step-strain experiments are modest, i.e. 3, 6, and 8. Thus, the elasticity does not have time to attain its maximum effect. Consequently, for the testing conditions studied here, only the applied capillary number and the viscosity ratio affect the shape of the deformed droplet after a step strain.

CONCLUSIONS

The contribution of weak elasticity of the droplet-phase on droplet behavior after steady-state and startup of shear flow has been investigated for isolated droplets of polybutadiene "Boger fluid" in a Newtonian poly(dimethyl siloxane) matrix and for 20% blends of polybutadiene "Boger fluid" in poly(dimethyl siloxane) under conditions of equal viscosities of droplet and matrix fluids. At the same capillary number, the steady-state shape deformation for elastic droplets is less than for Newtonian droplets. The droplet fluid with the higher degree of droplet elasticity, as measured by the higher value of N_1 at high shear rates, deforms less. Correspondingly, the critical capillary number for droplet breakup increases with increasing elasticity of the droplet phase. The steady-state capillary number calculated from the volume-averaged droplet diameter of 20%-dispersed phase blends also increases when the droplet elasticity increases. However, the droplet size at steady state in the 20% blend is smaller than for an isolated droplet of the same dispersed phase and same matrix under identical shearing conditions. This result suggests that local increases in shear stress present in concentrated blends are more important than coalescence in influencing steady-state droplet size. Although weak elasticity of the droplet phase affects the steady-state droplet deformation, in startup of shear flow, the elasticity of the droplet does not affect the droplet shape, either during the startup of shear flow or during the relaxation process after the startup of shear flow.

ACKNOWLEDGEMENTS

W.L. and A.S. would like to acknowledge the fellowship provided by Thailand Research Fund (TRF) in the Royal Golden Jubilee Ph D. Program grant no. PHD/00144/2541, and the TRF-BRG grant no. BRG/12/2544.

REFERENCES

Almusallam, A. S., R. G. Larson and M. J. Solomon, "A constitutive model for the prediction of ellipsoidal droplet shapes and stresses in immiscible blends", *J. Rheol.* **44**, 1055-1083 (2000).

Boger, D. V. and R. J. Binnington, "Separation of elastic and shear thinning effects in the capillary rheometer", *Trans. Soc. Rheol.* **21**, 515-534 (1977).

Chaffey, C. E. and H. Brenner, "A second-order theory for shear deformation of drops", *J. Colloid Interface Sci.* **24**, 258-269 (1967).

Choi, S. J. and W. R. Schowalter, "Rheological properties of nondilute suspensions of deformable particles", *Phys. Fluids* **18**, 420-427 (1975).

De Bruijn, R. A., "Deformation and breakup of drops in simple shear flow", Ph.D.Thesis, Eindhoven University of Technology, 1989.

Doi, M. and T. Ohta, "Dynamics and rheology of complex interfaces", *J. Chem. Phys.* **95**, 1242-1248 (1991).

Elmendorp, J. J. and R. J. Maalcke, "A study on polymer blending microrheology: Part 1", *Polym Eng. Sci.* **25**, 1041-1047 (1985).

Elmendorp, J. J.,"A study on polymer blending microrheology", *Polym Eng. Sci.* **26**, 418-426 (1986).

Frankel, N. A. and A. Acrivos, "The constitutive equation for a dilute emulsion", *J. Fluid Mech.* **44**, 65-78 (1970).

Grace, H. P., "Dispersion phenomena in high viscosity immiscible fluid systems and application of static mixers as dispersion devices in such systems", *Chem. Eng. Commun.* **14**, 225-277 (1982).

Graebling, D., R. Muller, and J. F. Palierne, "Linear viscoelastic behavior of some incompatible polymer blends in the melt. Interpretation of data with a model of emulsion of viscoelastic liquids", *Macromolecules* **26**, 320-329 (1993).

Grizzuti, N., G. Buonocore, and G. Iorio, "Viscous behavior and mixing rules for an immiscible model polymer blend", *J. Rheol.* **44**, 149-164 (2000).

Guido, S. and M. Villone, "Three-dimensional shape of a drop under simple shear flow", *J. Rheol.* **42**, 395-415 (1998).

Guido, S., M. Minale, and P. L. Maffettone, "Drop shape dynamics under shear-flow reversal", *J. Rheol.* **44**, 1385-1399 (2000).

Hayashi, R., M. Takahashi, H. Yamane, H. Jinnai, and H. Watanabe, "Dynamic interfacial properties of polymer blends under large step strains: shape recovery of a single droplet", *Polymer* **42**, 757-764 (2001a).

Hayashi, R., M. Takahashi, T. Kajihara, and H. Yamane, "Application of large double-step shear strains to analyze deformation and shape recovery of a polymer droplet in an immiscible polymer matrix", *J. Rheol.* **45**, 627-639 (2001b).

Jansen, K. M. B., W. G. M. Agterof, and J. Mellema, "Droplet breakup in concentrated emulsions", *J. Rheol.* **45**, 227-236 (2001).

Janssen, J. M. H., "Dynamics of liquid-liquid mixing", Ph. D. Thesis, TU Eindhoven, 1993.

Jansseune, T., J. Mewis, P. Moldenaers, M. Minale, P. L. Maffettone, "Rheology and rheological morphology determination in immiscible two-phase polymer model blends", *J. Non-Newtonain Fluid Mech.* **93**, 153-165 (2000).

Kennedy, M. R., C. Pozrikidis, and R. Skalak, "Motion and deformation of liquid drops, and the rheology of dilute emulsions in simple shear flow", *Comput. Fluids* **23**, 251-278 (1994).

Levitt, L., C. W. Macosko and S. D. Pearson, "Influence of normal stress difference on polymer drop deformation", *Polym. Eng. Sci.* **36**, 1647-1655 (1996).

Luciani, A., M. F. Champagne, L. A. Utracki, "Interfacial tension coefficient from the retraction of ellipsoidal drops", *J. Polym. Sci. Pol. Phys.* **35**, 1393-1403 (1997).

Mighri, F., A. Ajji, and P. J. Carreau, "Influence of elastic properties on drop deformation in elongational flow", *J. Rheol.* **41**, 1183-1201 (1997).

Mighri, F., P. J. Carreau, and A. Ajji, "Influence of elastic properties on drop deformation and breakup in shear flow" *J. Rheol.* **42**, 1477-1490 (1998).

Minale, M., P. Moldenaers, and J. Mewis, "Effect of shear history on the morphology of immiscible polymer blends", *Macromolecules* **30**, 5470-5475 (1997).

Mo, H., C. Zhou, and W. Yu, "A new method to determine interfacial tension from the retraction of ellipsoidal drops", *J. Non-Newtonian Fluid Mech.* **91**, 221-232 (2000).

Okamoto, K., M. Takahashi, H. Yamane, H. Kashihara, H. Watanabe and T. Masuda, "Shape recovery of a dispersed droplet phase and stress relaxation after application of step shear strains in a polystyrene/polycarbonate blend melt", *J. Rheol.* **43**, 951-965 (1999).

Palierne, J. F., "Linear rheology of viscoelatic emulsions with interfacial tension", *Rheol. Acta* **29**, 204-214 (1990).

Sundararaj, U., and C. W. Macosko, "Drop breakup and coalescence in polymer blends: the effects of concentration and compatibilization", *Macromolecules,* **28,** 2647-2657 (1995).

Taylor, G. I., "The viscosity of a fluid containing small drops of another fluid", *Proc. R. Soc. London*, Ser. A **138**, 41-48 (1932).

Taylor, G. I., "The formation of emulsions in definable fields of flow", *Proc. R. Soc. London*, Ser. A **146**, 501-523 (1934).

Tsakalos, V. T., P. Navard, and E. Peuvrel-Disdier, "Deformation and breakup mechanisms of single drops during shear", *J. Rheol.* **42**, 1403-1417 (1998).

Uijittewaal, W. S. J. and E. J. Nijhof, "The motion of a droplet subjected to linear shear flow including the presence of a plane wall", *J. Fluid Mech.* **302**, 45-63 (1995).

Wu, S., "Phase structure and adhesion in plymer blends: A criterion for rubber toughening", *Polymer* **26**, 1855-1863 (1985).

Xing, P., M. Bousmina, and D. Rodrigue, "Critical experimental comparison between five techniques for the determination of interfacial tension in polymer blends: model system of polystyrene/polyamide-6", *Macromolecules* **33**, 8020-8034 (2000).

Yamane, H., M. Takahashi, R. Hayashi, K. Okamoto, H. Kashihara and T. Masuda, "Observation of deformation and recovery of poly(isobutylene) droplet in a poly(isobutylene)/poly(dimethyl siloxane) blend after application of step shear strain", *J. Rheol.* **42**, 567-580 (1998).

TABLES

TABLE 2.1. Molecular weight and specific gravity of blend components

Component	M_n (g/mol)	Specific gravity At 25°C
PDMS	139 000	0.97
Ricon150 (polybutadiene)	3900	0.89

Table 2.2. The constituent components, testing temperature, viscosity ratio (η_r), interfacial tension (Γ), stress ratio of dispersed phase (S_{Rd}), stress ratio of matrix phase (S_{Rm}) at a shear rate of 10 s^{-1}, effective relaxation time of dispersed phase ($\tau_{eff,d}$), and effective relaxation time of high-molecular weight polymer component of dispersed phase ($\tau_{eff,p,d}$).

Blend	Constituent Components (Matrix Phase : Dispersed Phase)	Testing Temp. (°C)	η_r	Γ (mN/m)	S_{Rm} at 10 s^{-1}	S_{Rd} At 10 s^{-1}	$\tau_{eff,d}$ (s)	$\tau_{eff,p,d}$ (s)
A1	PDMS : Pure Ricon	21.0	1	3.17	0.12	0	0.002	-
A2	PDMS : 0.1% high MW PBd solution	21.5	1	3.20	0.13	0.15	0.02	0.51
A3	PDMS : 0.2% high MW PBd solution	21.8	1	3.23	0.12	0.29	0.04	0.48
A4	PDMS : 0.5% high MW PBd solution	23.5	1	2.92	0.10	0.66	0.12	0.41
B1	PDMS : Pure PBd	29.5	0.5	2.95	0.08	0		
B3	PDMS : 0.2% high MW PBd solution	30.5	0.5	2.81	0.07	0.21		
B4	PDMS : 0.5% high MW PBd solution	33.0	0.5	2.87	0.07	0.47		

TABLE 2.3. Parameters for droplet relaxation experiments.

Blend	Gap (μm)	r_0 (μm)	Ca	$\dot{\gamma}_{applied}$ (s^{-1})	$\gamma_{applied}$
A1	1700	99	11 , 15 , 20 , 24	3.5 , 4.8 , 6.4 , 7.8	2.2, 3.0, 4.1, 5.0
A2	1800	106	11 , 15 , 20 , 24	3.3 , 4.6 , 6.1 , 7.4	2.2, 3.0, 4.1, 5.0
A3	1800	100	11 , 15 , 20 , 24	3.5 , 4.8 , 6.5 , 7.8	2.2, 3.0, 4.1, 5.0
A4	1800	115	11 , 15 , 20 , 24	2.9 , 3.9 , 5.3 , 6.4	2.2, 3.0, 4.1, 5.0

TABLE 2.4. The matrix-phase viscosity, the blend viscosities predicted by the FA model, and the measured blend viscosity at various shear rates, as well as the steady-state capillary number (Ca_{ss}) calculated based on each corresponding viscosity for blend A1.

	Shear rate (s^{-1})				
	0.3	0.5	0.7	1.0	2.0
D_v (μm)	55.0	34.0	25.6	19.2	10.9
Matrix viscosity (Pa.s)	102.2	102.0	101.7	101.6	101.3
Blend viscosity predicted by FA model (Pa.s)	117.4	116.6	115.6	114.3	112.0
Measured blend viscosity (Pa.s)	138.9	136.7	134.9	133.6	129.0
Ca_{ss} calculated from matrix viscosity	0.266	0.274	0.287	0.307	0.349
Ca_{ss} calculated from blend viscosity predicted by FA model	0.306	0.313	0.326	0.345	0.386
Ca_{ss} calculated from measured value of blend viscosity	0.361	0.367	0.381	0.404	0.444

I21615627

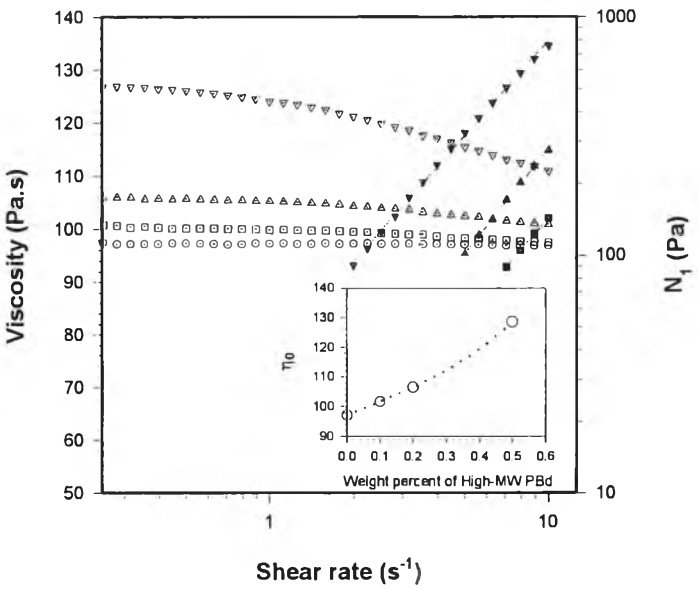

Figure 2.1 The dependence of viscosity and first normal stress difference on shear rate for pure Ricon PBd, and for Boger solutions of Ricon containing 0.1%, 0.2%, and 0.5% high-MW PBd at 21.0 ^{0}C. Insert: the dependence of zero-shear viscosity on concentration of high-molecular-weight PBd in PBd Boger fluids

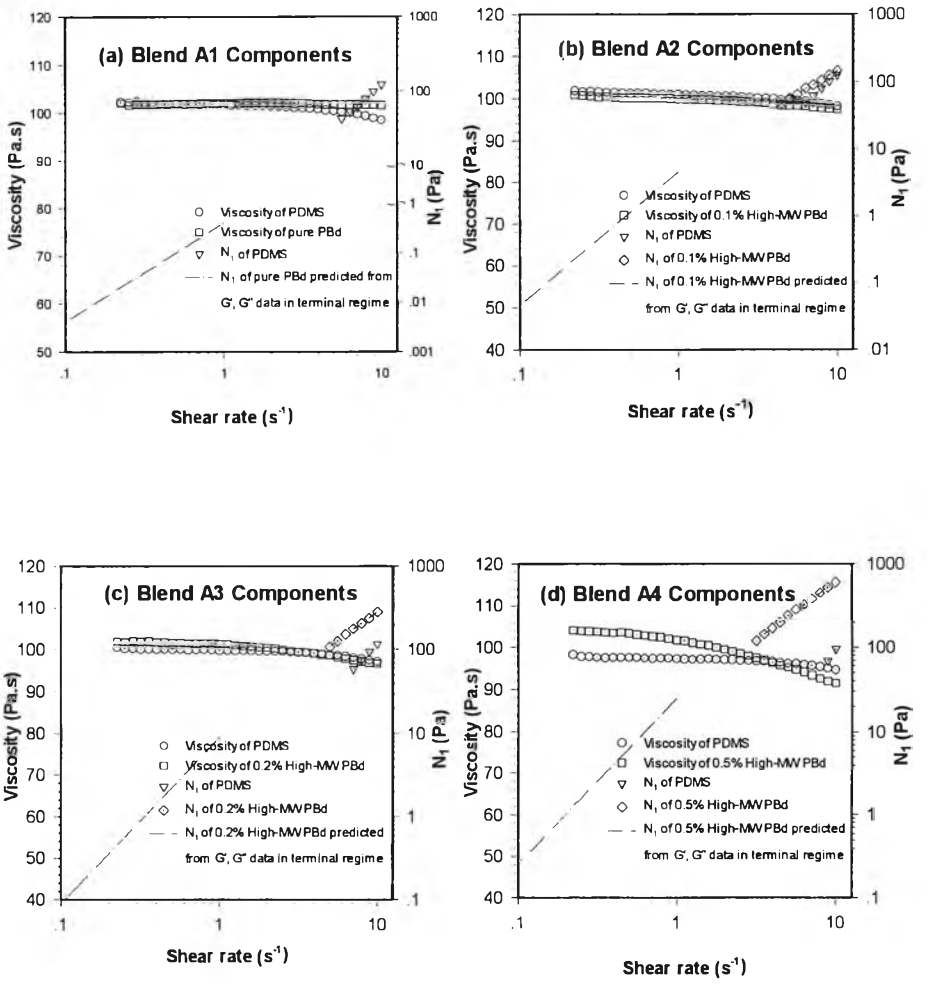

Figure 2.2 The steady shear viscosity and first normal stress difference of the droplet and matrix phases of blends (a) A1, (b) A2, (c) A3, and (d) A4 at the temperatures at which the matrix and droplet fluid have the same viscosity

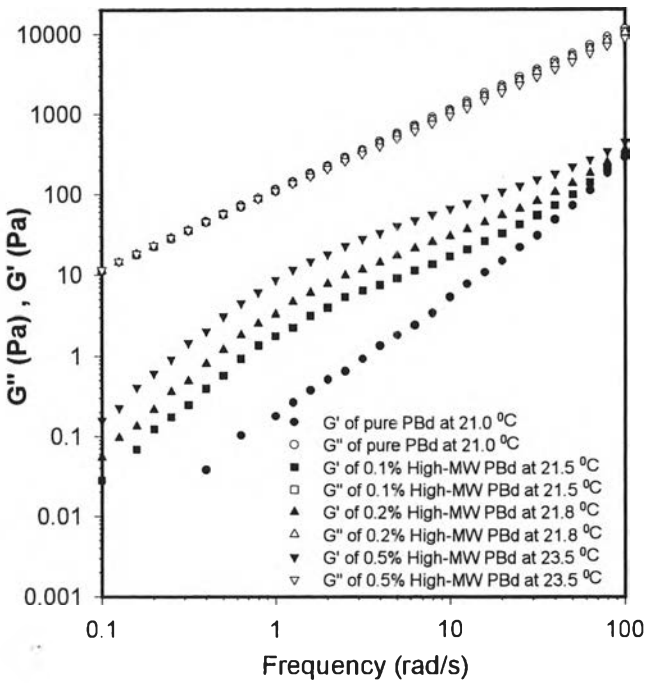

Figure 2.3 The dependence of storage modulus (G') and loss modulus (G") on frequency for all dispersed-phase fluids studied

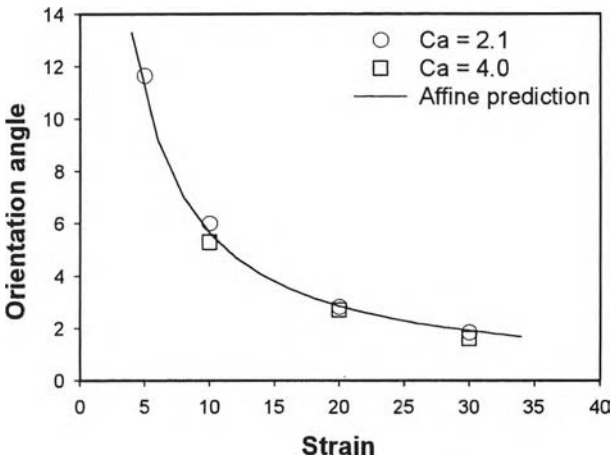

Figure 2.4 Droplet orientation angle obtained from rheological measurements after startup of steady shear and the angle predicted from affine deformation

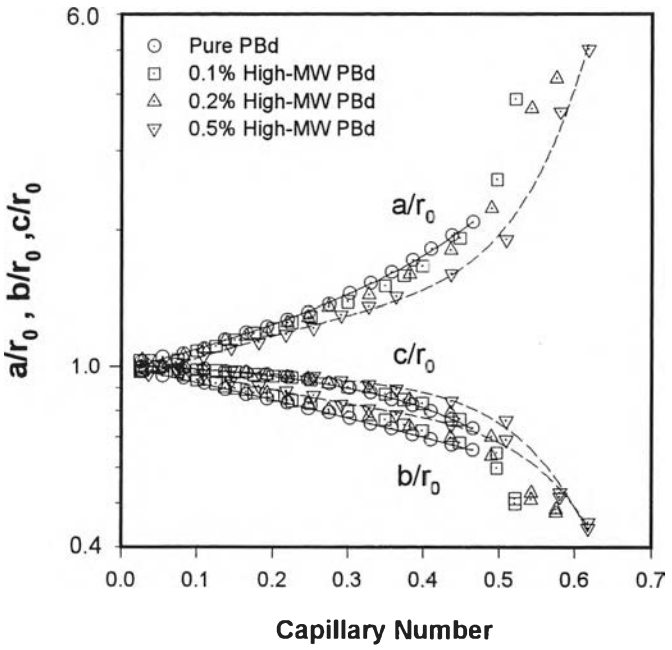

Figure 2.5 The dependences of the steady-state half-lengths of the three principal axes on applied capillary number of all blends studied. The solid lines were drawn to guide the eye through the data points for the pure PBd and the 0.5% High-MW PBd

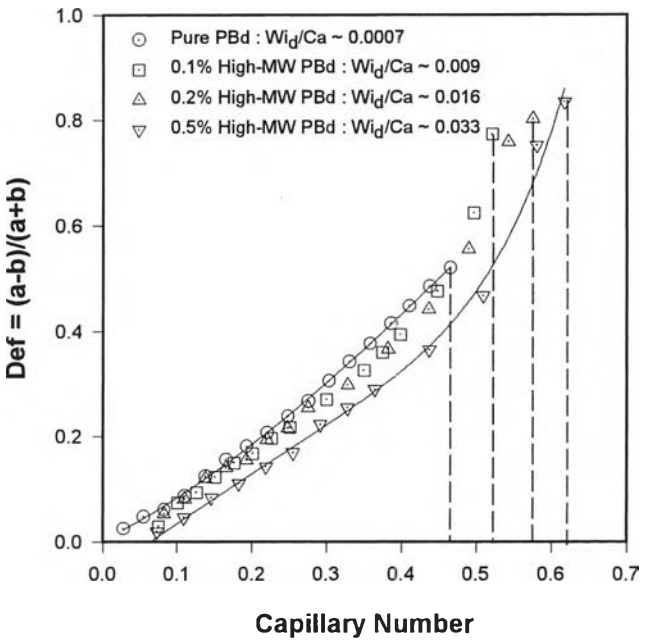

Figure 2.6 The dependence of steady-state deformation parameter on applied capillary number of all blends studied. The dashed and dotted lines indicate the critical capillary number for each fluid system. The solid lines were drawn to guide the eye through the data points for the pure PBd and the 0.5% High-MW PBd

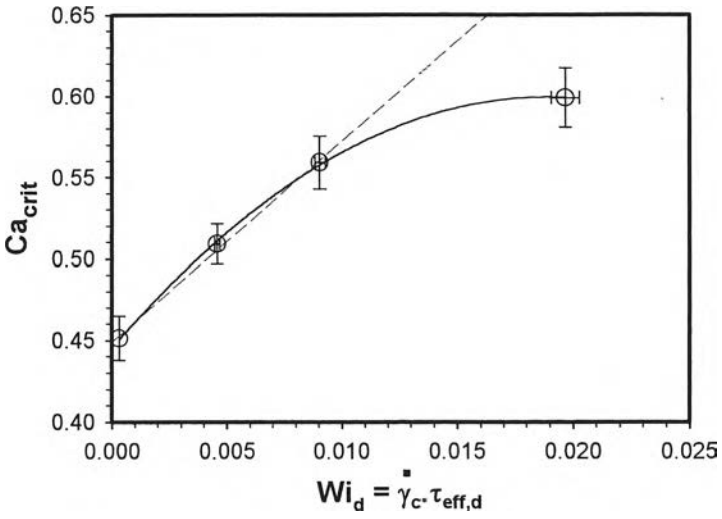

Figure 2.7 The dependence of critical capillary number (Ca_{crit}) with droplet-phase Weissenberg number (Wi_d) estimated from the G' and G" data at terminal regime

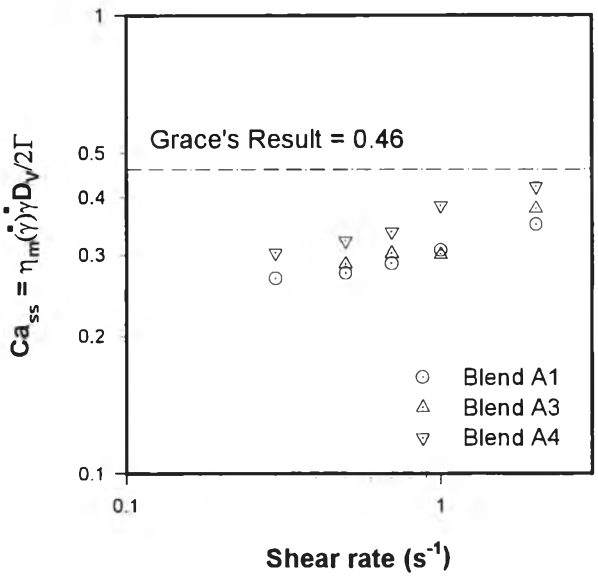

Figure 2.8 The dependence of steady-state capillary number on shear rate calculated from matrix phase viscosity and volume-averaged diameters for 20% dispersed-phase blends, in prolonged shearing for a strain of 20,000 units after a step-up in shear rate from a previous shear rate

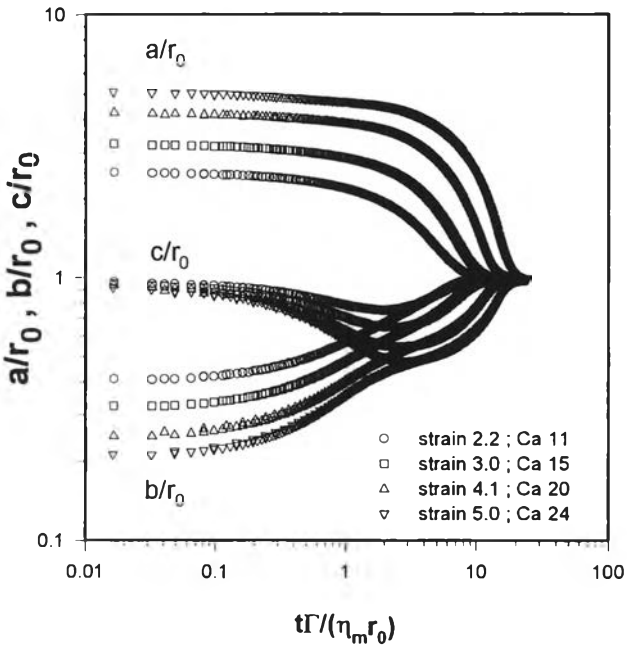

Figure 2.9 The dependences of the half-lengths of the three principle axes normalized by original droplet radius on time normalized by $\Gamma/\eta_m r_0$ for fluid system A1

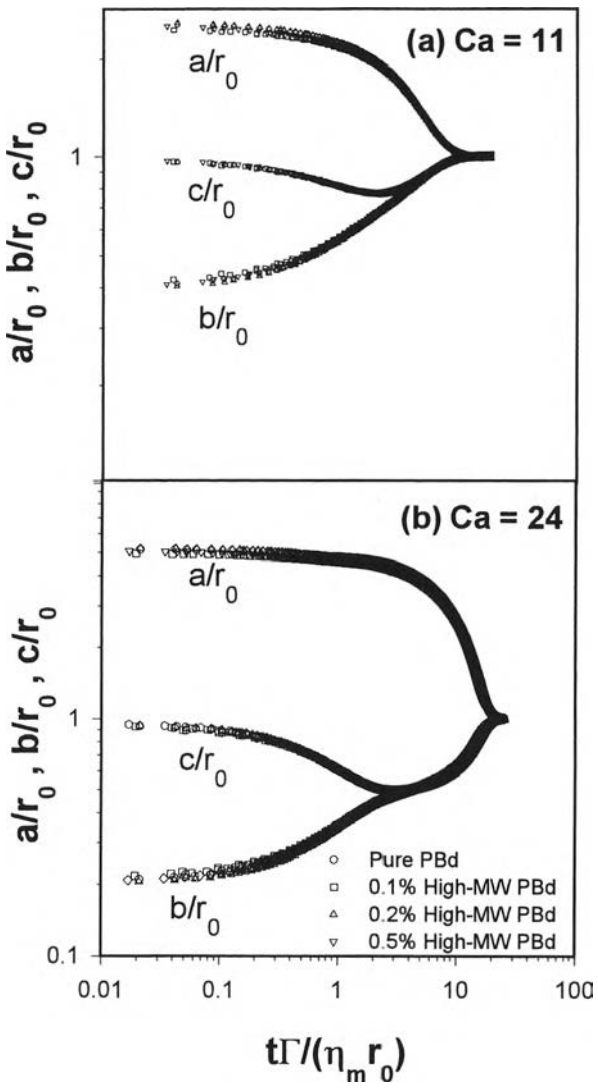

Figure 2.10 The dependences of the half-lengths of the three principle axes normalized by original droplet radius on time normalized by $\Gamma/\eta_m r_0$ at applied Ca of (a) 11 and (b) 24 for all blends

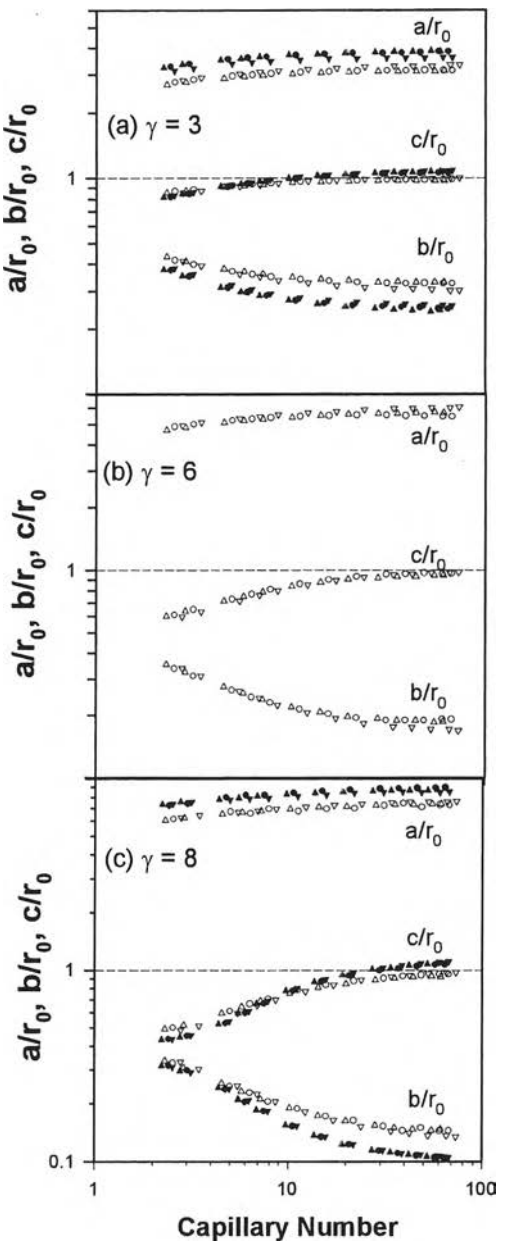

Figure 2.11 The dependences of the half-lengths of the three principal axes on applied capillary number at strains of (a) 3, (b) 6, and (c) 8 for blends A1 (○), B1 (●), A3 (Δ), B3 (▲), A4 (∇), and B4 (▼). The open symbols represent blends with viscosity ratio of unity, while the closed symbols represent blends with viscosity ratio of 0.5